Energy Proceedings
Vol 57, 2025
ISSN 2004-2965

Numerical Simulation of CO_2 Plume Migration in the Tiaohu Formation Saline Aquifer, Santanghu Basin, China

Danhe Fu [1], Yu Liu [1,2*]
1 Key Laboratory of Ocean Energy Utilization and Energy Conservation Ministry of Education, School of Energy and Power Engineering, Dalian University of Technology, Dalian,116024, China
2 Ningbo Institute of Dalian University of Technology, Ningbo,315211, China
([*]Corresponding author: liuyu@dlut.edu.cn)

ABSTRACT

Deep saline aquifers remain a critical option for large-scale CO_2 storage to mitigate global climate change. The Permian saline aquifer in the Tiaohu Formation of the Santanghu Basin has emerged as an ideal target for CO_2 geological sequestration due to its superior storage conditions. This study employs the ECO2N module within the TOUGH2-PetraSim software to establish a numerical model of multiphase flow in a basalt-tuff reservoir system. The research reveals the fluid migration characteristics following CO_2 injection into the saline aquifer, with a focus on analyzing the influence of well orientation on CO_2 plume migration, including the variation patterns of CO_2 gas saturation and solubility. Research demonstrates that horizontal wells enable more uniform spatial distribution of CO_2.

Keywords: CO_2 geological sequestration, Santanghu Basin, numerical simulation

NONMENCLATURE

Symbols	
M	Mass accumulation
F	Mass flux
q	Source/sink
t	Time
∇·	Divergence
∇	Gradient
S	Saturation
X	Mass fraction
ϕ	Porosity
ρ	Density (kg/m^3)
k_{rg}	Relative gas permeability
k_{rl}	Relative liquid permeability
p	Pressure (Pa)
Subscripts/superscripts	
k	Component
w	Water
l	Liquid phase
g	Gas phase
s	Solid phase
c	CO_2 component

1. INTRODUCTION

The significant climate warming caused by global greenhouse gas emissions has become a major challenge of our era[1]. Carbon Capture and Storage (CCS) technology, as one of the most promising solutions to address emissions, involves separating and purifying CO_2 from industrial sources (e.g., power plants, refineries), transporting it via pipelines/ships to storage sites, and injecting it into geological formations for permanent isolation[2]. Suitable geological structures for CO_2 subsurface storage include depleted oil and gas reservoirs, deep saline aquifers, and unmineable coal seams[3][4]. Among these, deep saline aquifers are globally widespread, highly accessible, and possess enormous storage potential[2][5][6]. Currently, there are over 16 planned or operational CO_2 injection projects in saline aquifers worldwide, encompassing both geological storage and CO_2-enhanced water recovery (CO_2-EWR), ranging from large-scale projects (>1 Mt/year) to small-scale integrated demonstration initiatives. Notable examples include Norway's Snøhvit CO_2 Storage Project (operational since 2008), Algeria's in Salah Storage Project (launched in 2004), and China's Shenhua CCS Demonstration Project[7][8][9]. The Chinese government has integrated the "Carbon Peak" and "Carbon Neutrality" goals into its ecological civilization strategy, making the advancement of CO_2 geological storage and utilization technologies a

This is a paper for International CCUS Conference 2025 (ICCUSC 2025), May 28-29, 2025, Beijing, China.

critical pathway for future emissions reduction and energy security[10][11]. According to domestic and international studies, China's CCUS (Carbon Capture, Utilization, and Storage) mitigation demand under carbon neutrality targets is projected to be 0.2–408 million tons by 2030, 600 million–1.45 billion tons by 2050, and 1–1.82 billion tons by 2060[12].

Recent studies by multiple researchers indicate that the orientation of injection wells significantly impacts storage efficiency and plume migration control. While vertical wells have long been the conventional approach, horizontal wells are increasingly being adopted in geological storage projects due to their multiple advantages over vertical wells, with only marginal additional cost increments[13]. Horizontal wells can reduce bottomhole pressure, improve pressure distribution, and delay CO_2 plume migration toward the caprock. The extended reach of horizontal wells facilitates more uniform pressure dispersion, thereby mitigating fracturing risks and potential CO_2 leakage[14].

The Santanghu Basin is located in the northeastern part of Xinjiang, stretching in a NW-SE direction with a total area of 2.3×10^4 km². The Malang-Tiaohu Depression within the basin serves as the primary exploration target for unconventional Permian oil reservoirs[15]. Numerical simulation can predict migration processes over centennial or even millennial timescales. Therefore, this study establishes a multiphase flow coupling model for CO_2 sequestration in saline aquifers using the ECO2N module of the TOUGH2-Petrasim software, focusing on revealing the influence of injection well orientation on the spatial-temporal evolution patterns of CO_2 plume saturation and dissolution.

2. MODEL SETUP AND SIMULATION PARAMETERS

2.1 Model geometry

Based on the actual stratigraphic structure of the Tiaohu Formation in the Santanghu Basin, this study established the geometric model shown in Fig. 1. In accordance with the key technology development project for CO_2 utilization under carbon neutrality goals, the simulation assumes an annual CO_2 injection of 1 million tons into the aquifer, with a simulation period set at 100 years. This duration is sufficient to observe the migration patterns of the CO_2 plume and the spatial distribution of dissolved CO_2.

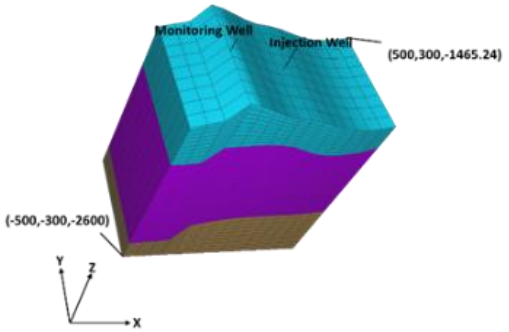

Fig. 1. Three-dimensional geological model of the Tiaohu Formation in Santanghu Basin

2.2 Initial conditions

The material properties, initial reservoir conditions, and injection parameters used in the simulation model are detailed in Table 1. Both the upper and lower boundaries of the storage formation consist of tuff. This study employs experimentally measured rock sample data from well M56-15H in the Tiaohu Formation of the Malang Sag, Santanghu Basin. Based on classical projects, the porosity ranges between 10%-35%, while permeability varies from 10 mD to 4000 mD[16]. Accordingly, the reservoir permeability in this study is set at 100 mD. Other key parameters (including specific heat capacity, thermal conductivity, and compressibility) are derived from reliable data sources adopted in classical simulation studies [17].According to drilling and pressure test results, the initial reservoir temperature gradient is 2.946°C/100m with a pressure coefficient of 1.137[18]. The initial formation conditions are established as fully water-saturated state.

Table 1 Material properties, initial reservoir conditions and injection parameters used in the simulation model

Formation	
Tuff density	2700 kg/m³
Basalt density	3000 kg/m³
Tuff porosity	14.2%
Basalt porosity	16.5%
Tuff permeability	5.92×10^{-16} m²
Basalt permeability	9.87×10^{-14} m²
Specific heat capacity	2.0 W/(m·K)
Thermal conductivity	1000 J/(kg·K)
Compressibility	4.5×10^{-10} Pa^{-1}
Initial Reservoir Conditions	
Initial reservoir pressure	Hydrostatic
CO_2 partial pressure	0 MPa
Temperature gradient	2.8 °C/100m
Salinity	0.01 (mass fraction)
Injection Parameters	
CO_2 injection rate	13.89 kg/s
CO_2 injection enthalpy	493 kJ/kg

Total CO_2 injected	100 million tons
Injection duration	10 years
Simulation period	100 years

2.3 Mathematical model of CO_2-water-NaCl system

The coupled system of partial differential equations governing isothermal two-phase flow in deformable porous media under fully saturated conditions is presented below:

$$\frac{\partial M^k}{\partial t} = -\nabla \cdot F^k + q^k \quad (1)$$

where M mass accumulation (kg/m^3), F mass flux (kg/(m^2·s), q source/sink term (kg/m^3·s), t time (s), ∇ divergence, superscript k denotes any one of the mass components for CO_2, water, air, etc.

Taking the water component in the fluid as an example, its governing equation is expressed as follows:

$$\frac{\partial}{\partial t}\left(\phi\left(X_l^w S_l \rho_l + X_g^w S_g \rho_g\right)\right) = -\nabla \cdot \left\{X_l^w \rho_l \left(-k\frac{k_{rl}}{\mu_l}(\nabla P_l - \rho_l g)\right) + X_g^w \rho_g \left(-k\frac{k_{rg}}{\mu_g}\left(\nabla P_g - \rho_g g\right)\right)\right\} + \left(q_1^w + q_g^w\right) \quad (2)$$

where, in Eq. (2), the symbols: S saturation, X mass fraction, ϕ porosity, ρ density (kg/m^3), k permeability (m^2), k_{rg} relative gas permeability, k_{rl} relative liquid permeability, P pressure (Pa), superscripts: w stands for water, subscripts: l liquid phase; g gas phase; s solid phase.

For the CO_2 component in the fluid, the governing equation can be expressed as:

$$\frac{\partial}{\partial t}\left(\phi\left(X_l^c S_l \rho_l + X_g^c S_g \rho_g\right)\right) = -\nabla \cdot \{X_l^c \rho_l \left(-k\frac{k_{rl}}{\mu_l}(\nabla P_l - \rho_l g) + X_g^c \rho_g \left(-k\frac{k_{rg}}{\mu_g}\left(\nabla P_g - \rho_g g\right)\right)\right\} + \left(q_l^c + q_g^c + q_s^c\right) \quad (3)$$

where, superscripts: c denotes CO_2.

2.4 Parameters used in simulation

This study utilizes the ECO2N module of the TOUGH2 software for numerical simulations. Developed specifically for CO_2 geological storage in saline aquifers, this module provides a comprehensive description of the thermodynamic and thermophysical properties of the H_2O-NaCl-CO_2 system under specified operating conditions, including a temperature range of 10-110°C, pressures below 600 bar, and salinity levels up to halite saturation. Prior to conducting numerical simulations, all relevant parameters must be properly configured in the TOUGH2 software according to specific engineering requirements. For CO_2 geological storage applications, the H_2O-NaCl-CO_2 system exhibits particularly complex thermodynamic characteristics. The density, viscosity, and solubility of CO_2 in brine are all functions of pressure and temperature[19][20], while capillary pressure and relative permeability are described using the van Genuchten model[21]. In this study, the residual gas saturation was set to 0.1 and the irreducible water saturation to 0.15, serving as fundamental parameters for calculating relative permeability curves. These settings reflect the complex multiphase flow behavior expected during CO_2 injection and migration in deep saline formations, where the interplay of thermodynamic properties and rock-fluid interactions significantly influences storage efficiency and long-term containment security. The selected parameters align with experimental data and field observations from analogous CO_2 storage projects, ensuring physically realistic simulation results.

3. RESULTS AND DISCUSSION

3.1 Comparative analysis of CO_2 saturation between vertical and horizontal wells of equal length

To elucidate the impact of well orientation on CO_2 storage efficiency, we first investigated the underlying mechanisms. A comparative analysis was conducted between horizontal wells and vertical wells, with the horizontal well completion depth maintained at the same elevation as the bottom of the vertical well. CO_2 injection via horizontal wells yields significantly greater lateral migration distances compared to vertical wells, with the migration distance increasing proportionally to wellbore length (Fig. 2 and Fig. 3)

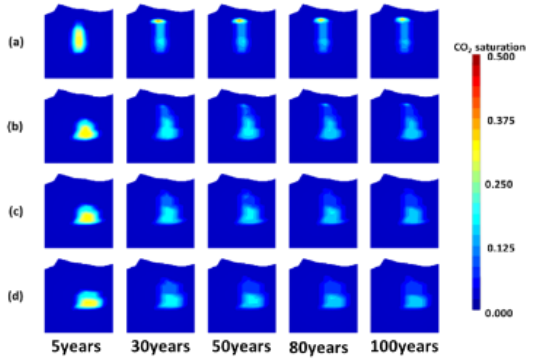

Fig. 2. CO_2 saturation contour maps in the X-Z plane over time: (a) Vertical well, (b) 200-m horizontal well, (c) 250-m horizontal well, (d) 300-m horizontal well

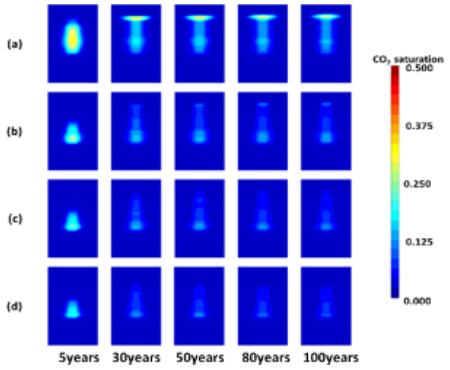

Fig. 3. CO_2 saturation contour maps in the Y-Z plane over time: (a) vertical well, (b) 200-m horizontal well, (c) 250-m horizontal well, (d) 300-m horizontal well

The CO_2 saturation from vertical wells first reaches the reservoir top, with the 200-m horizontal well achieving top contact after 10 years, while other horizontal well configurations fail to reach the top within the 100-year simulation period (Fig. 4 and Fig. 9). Downhole monitoring data reveal the lowest CO_2 saturation occurs in vertical wells, whereas the 200-m horizontal well exhibits the maximum bottomhole saturation (Fig. 6 and Fig. 7). Notably, vertical wells demonstrate significantly higher top-zone CO_2 saturation (0.38) compared to horizontal wells. The horizontal wells show a decreasing trend in top-zone saturation with increasing well length, a distribution characteristic that enhances long-term storage potential (Fig. 5 and Fig. 8).

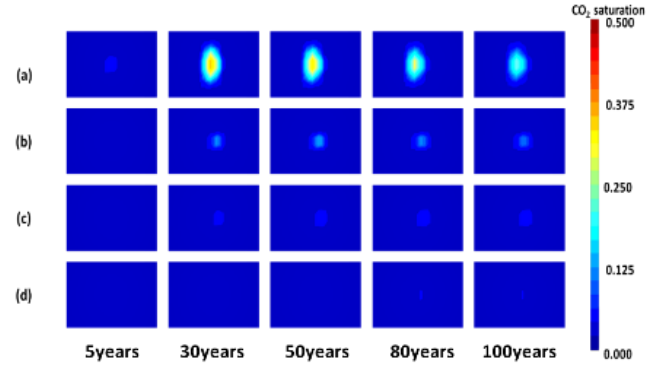

Fig. 4. Temporal evolution of CO_2 saturation contours in the X-Y plane at the reservoir top: (a) vertical well, (b) 200-m horizontal well, (c) 250-m horizontal well, (d) 300-m horizontal well

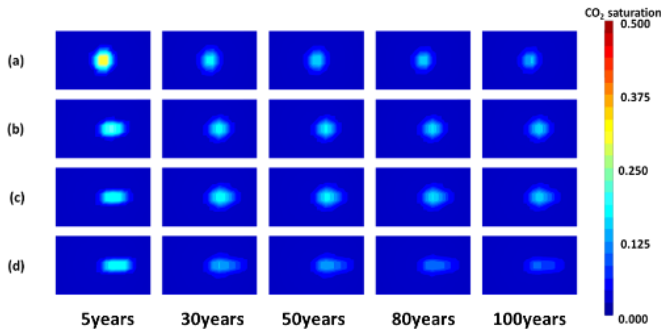

Fig. 5. Temporal evolution of CO_2 saturation contours in the X-Y plane at wellhead elevation: (a) vertical well, (b) 200-m horizontal well, (c) 250-m horizontal well, (d) 300-m horizontal well

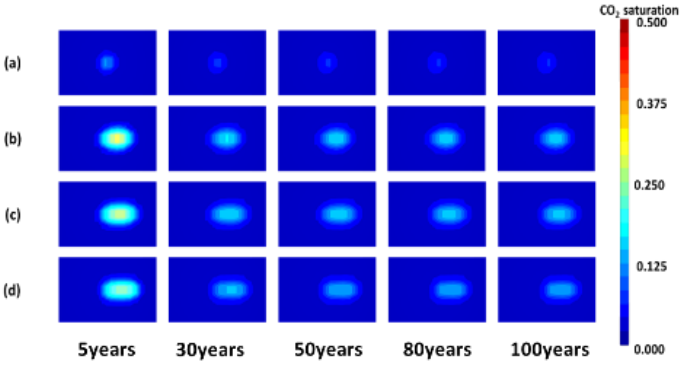

Fig. 6. Temporal evolution of CO_2 saturation contours in the X-Y plane at well bottom depth: (a) vertical well, (b) 200-m horizontal well, (c) 250-m horizontal well, (d) 300-m horizontal well

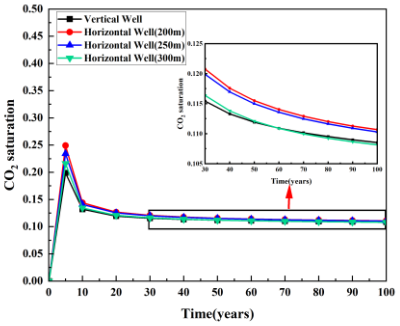

Fig. 7. Time-series line plot of CO_2 saturation at well bottom

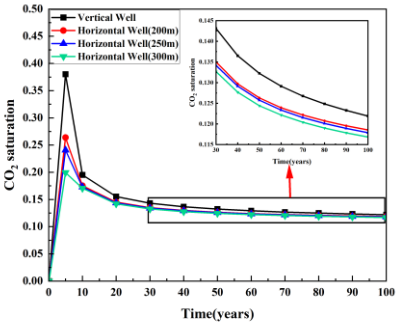

Fig. 8. Time-series line plot of CO_2 saturation at wellhead elevation

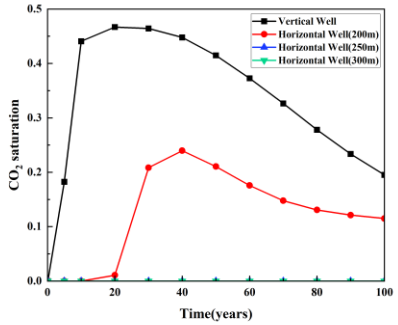

Fig. 9. Time-series line plot of CO_2 saturation at the reservoir top

3.2 Comparative analysis of CO_2 solubility between vertical and horizontal wells of equal length

Fig. 10 and Fig. 11 demonstrate that vertical wells exhibit a distinct vertical gradient distribution of CO_2 solubility, while horizontal wells display a more uniform dissolution pattern along the horizontal plane.

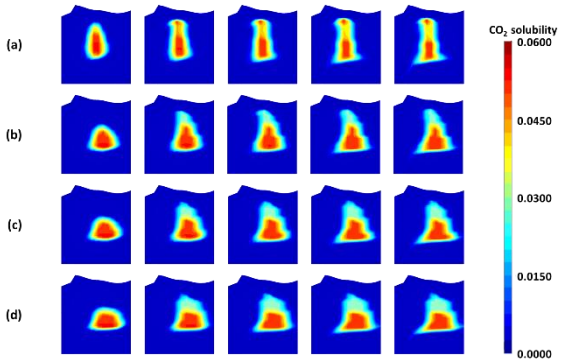

Fig. 10. CO_2 Solubility Contour Maps in the X-Z Plane Over Time: (a) Vertical Well, (b) 200-m Horizontal Well, (c) 250-m Horizontal Well, (d) 300-m Horizontal Well

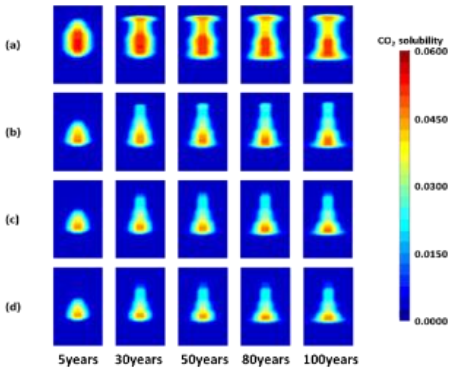

Fig. 11. CO_2 solubility contour maps in the Y-Z plane over time: (a) Vertical well, (b) 200-m horizontal well, (c) 250-m horizontal well, (d) 300-m horizontal well

Further analysis (Fig. 12 and Fig. 17) reveals that vertical wells achieve higher localized solubility enrichment at the reservoir top, with both vertical wells and 200-m horizontal wells reaching peak solubility values of 0.05 in this zone. Notably (Fig. 13 and Fig. 16), although horizontal wells of varying lengths show comparable solubility values (0.051) at the wellhead position, increased well length significantly enhances the spatial extent of CO_2 dissolution. Downhole monitoring data (Fig. 14 and Fig. 15) indicate that while longer horizontal wells provide greater dissolution coverage at the well bottom, all four well configurations attain similar solubility magnitudes in this region.

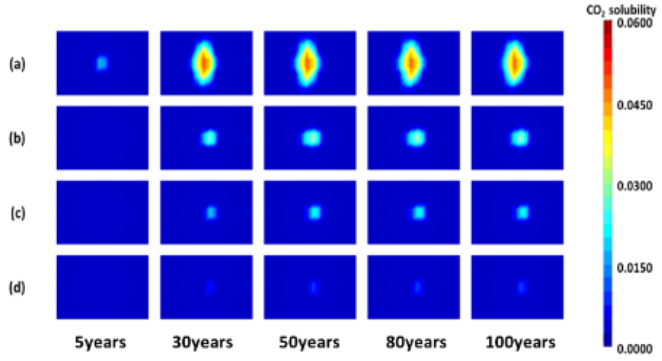

Fig. 12. Temporal evolution of CO_2 solubility contours in the X-Y plane at the reservoir top: (a) Vertical well, (b) 200-m horizontal well, (c) 250-m horizontal well, (d) 300-m horizontal well

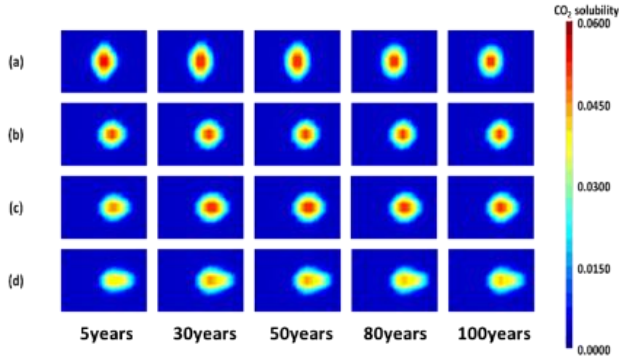

Fig. 13. Temporal evolution of CO_2 solubility contours in the X-Y plane at wellhead elevation: (a) Vertical well, (b) 200-m horizontal well, (c) 250-m horizontal well, (d) 300-m horizontal well

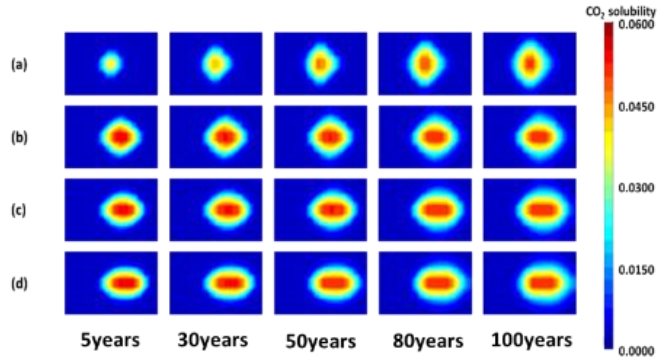

Fig. 14. Temporal evolution of CO_2 solubility contours in the X-Y plane at well bottom depth: (a) Vertical well, (b) 200-m horizontal well, (c) 250-m horizontal well, (d) 300-m horizontal well

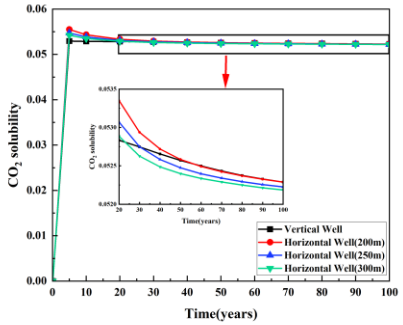

Fig. 15. Time-series line plot of CO_2 solubility at well bottom

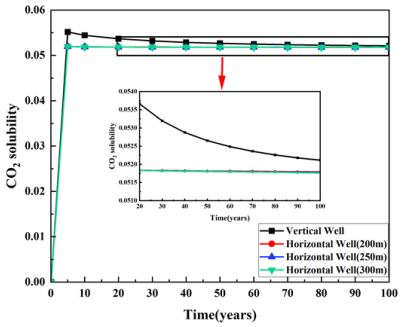

Fig. 16. Time-series line plot of CO_2 solubility at wellhead elevation

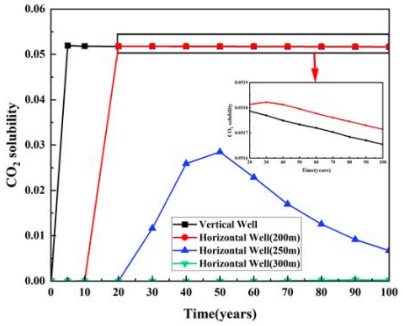

Fig. 17. Time-series line plot of CO_2 solubility at the reservoir top

4. CONCLUSIONS

Vertical wells enable rapid CO_2 migration to the reservoir top with high saturation accumulation (0.38), while 200-m horizontal wells develop maximum bottomhole saturation and exhibit decreasing top-zone saturation with increasing well length. This complementary distribution pattern demonstrates: vertical wells are optimal for short-term rapid storage, whereas horizontal wells provide superior long-term containment stability.

Vertical wells achieve higher CO_2 dissolution enrichment at the reservoir top (peak value: 0.05), while horizontal wells significantly expand the dissolution distribution range through increased wellbore length. However, all wells demonstrate comparable dissolution levels at the bottom, indicating that vertical wells are more conducive to localized dissolution trapping, whereas horizontal wells enable more uniform spatial distribution of CO_2.

REFERENCE

[1] Seneviratne, S. I., Donat, M. G., Pitman, A. J., Knutti, R., & Wilby, R. L. (2016). Allowable CO_2 emissions based on regional and impact-related climate targets. Nature, 529(7587), 477–483. https://doi.org/10.1038/nature16542

[2] IPCC. 2005 Intergovernmental Panel on Climate Change Special Report on CO_2 Capture and Storage Cambridge, UK.

[3] Li, F., Zhang, Y., Zhang, X., et al. (2014). Research on the suitability evaluation method of CO_2 geological storage in deep saline aquifers. Journal of Glaciology and Geocryology, *36*(3), 649–660.

[4] Stefan Bachu, Sequestration of CO_2 in geological media: criteria and approach for site selection in response to climate change, Energy Conversion and Management, Volume 41, Issue 9,2000,Pages 953-970,ISSN 0196-8904. https://doi.org/10.1016/S0196-8904(99)00149-1.

[5] Stefan Bachu, Didier Bonijoly, John Bradshaw, Robert Burruss, Sam Holloway, Niels Peter Christensen, Odd Magne Mathiassen,CO_2 storage capacity estimation: Methodology and gaps, International Journal of Greenhouse Gas Control, Volume 1, Issue 4,2007,Pages 430-443,ISSN 1750-5836. https://doi.org/10.1016/S1750-5836(07)00086-2.

[6] Benson, S. M., & Cole, D. R. (2008). CO_2 sequestration in deep sedimentary formations. Elements, 4(5), 325-331. https://doi.org/10.2113/gselements.4.5.325

[7] Estublier, A., & Lackner, A. S. (2009). Long-term simulation of the Snøhvit CO_2 storage. Energy Procedia, 1(1), 3221-3228. https://doi.org/10.1016/j.egypro.2009.02.106

[8] Ringrose, P. S., Mathieson, A. S., Wright, I. W., Selama, F., Hansen, O., Bissell, R., Saoula, N., & Midgley, J. (2013). The In Salah CO_2 storage project: Lessons learned and knowledge transfer. Energy Procedia, 37, 6226–6236. https://doi.org/10.1016/j.egypro.2013.06.551

[9] Wu, X. (2014). Shenhua Group's carbon capture and storage (CCS) demonstration. Mining Report, 150(1-2), 81-84. https://doi.org/10.1002/mire.201400006

[10] ZHOU Tianjun, CHEN Xiaolong, ZHANG Wenxia, ZHANG Lixia. Climate change and carbon neutrality[J]. Chinese Journal of Nature, 2024, 46(1): 1-11.
[11] Rogelj, J., Popp, A., Calvin, K. V., Luderer, G., Emmerling, J., Gernaat, D., Fujimori, S., et al. (2018). Scenarios towards limiting global mean temperature increase below 1.5 °C. Nature Climate Change, 8(4), 325-332. https://doi.org/10.1038/s41558-018-0091-3
[12] Cai, B., Li, Q., Zhang, X., et al. (2021). China carbon capture, utilization and storage (CCUS) annual report (2021): Research on China's CCUS pathways [Report]. Environmental Planning Institute of Ministry of Ecology and Environment, Institute of Rock and Soil Mechanics of Chinese Academy of Sciences, and The Administrative Center for China's Agenda 21.
[13] Zhang, Z., & Agarwal, R. K. (2012). Numerical simulation and optimization of CO_2 sequestration in saline aquifers for vertical and horizontal well injection. Computational Geosciences, 16(4), 891-899. https://doi.org/10.1007/s10596-012-9293-3
[14] Firoozmand, H., & Leonenko, Y. (2024). Horizontal wells for enhanced CO_2 storage in saline aquifers. Energy & Fuels, 38(13), 11875-11890. https://doi.org/10.1021/acs.energyfuels.4c00909
[15] Liang, S., Luo, Q., Wang, R., Chen, X., Yang, B., Ma, Q., & Liang, H. (2019). Geological characteristics and exploration practice of unconventional Permian oil resources in the Santanghu Basin. China Petroleum Exploration, 24(5), 624-635. http://www.cped.cn/CN/10.3969/j.issn.1672-7703.2019.05.009
[16] Wang, C., Wang, Z., & Li, H. (2024). Numerical modelling of CO_2 injection and storage in low porosity and low permeability saline aquifers: A design for the Permian Shiqianfeng Formation in the Yulin area, Ordos Basin. Sustainability, 16(23), 10593. https://doi.org/10.3390/su162310593
[17] Pruess K, Oldenburg C, Moridis G (1999) TOUTH2 user's manual, version 2.0. In: Lawrence Berkeley Laboratory report LBNL43134, Berkeley.
[18] Zhang, N., Jiang, M., Deng, Q., et al. (2017). Application of staged fracturing technology in horizontal wells for tight oil in Tiaohu Formation, Santanghu Basin. *West-China Exploration Engineering, 29*(8), 37-40.
[19] Span, R., & Wagner, W. (1996). A new equation of state for carbon dioxide covering the fluid region from the triple-point temperature to 1100 K at pressures up to 800 MPa. Journal of Physical and Chemical Reference Data, 25(6), 1509-1596. https://doi.org/10.1063/1.555991
[20] Bachu, S. (2003). Screening and ranking of sedimentary basins for sequestration of CO_2 in geological media in response to climate change. Environmental Geology, 44(3), 277-289. https://doi.org/10.1007/s00254-003-0762-9
[21] van Genuchten, M. T. (1980). A closed-form equation for predicting the hydraulic conductivity of unsaturated soils. Soil Science Society of America Journal, 44(5), 892-898. https://doi.org/10.2136/sssaj1980.03615995004400050002x